Heralded Generation of Correlated Photon Pairs from CdS/CdSe/CdS Quantum Shells

Andrew Marder[1], Sean Smith[1], James Cassidy[2], Dulanjan Harankahage[2], Zhongjian Hu[3], Stephen Savoy[3], George C. Schatz[4], Mikhail Zamkov[2], Anton V. Malko[1]

[1]Department of Physics, The University of Texas at Dallas, Richardson, Texas 75080

[2]The Center for Photochemical Sciences and Department of Physics, Bowling Green State University, Bowling Green, Ohio 43403.

[3]Nanohmics Inc, 6201 E. Oltorf, Suite 400, Austin, TX, 78741, USA

[4]Department of Chemistry, Northwestern University, Evanston IL 60208

Corresponding authors: zamkovm@bgsu.edu; anton.malko@utdallas.edu

Abstract. Quantum information processing demands efficient quantum light sources (QLS) capable of producing high-fidelity single photons or entangled photon pairs. Single epitaxial quantum dots (QDs) have long been proven to be efficient sources of deterministic single photons; however, their production via molecular-beam epitaxy presents scalability challenges. Conversely, colloidal semiconductor QDs offer scalable solution processing and tunable photoluminescence but suffer from broader linewidths and unstable emissions. This leads to spectrally inseparable emission from exciton (X) and biexciton (XX) states, complicating the production of single photons and triggered photon pairs. Here, we demonstrate that colloidal semiconductor quantum shells (QSs) achieve significant spectral separation (~ 75-80 meV) and long temporal stability of X and XX emissive states, enabling the observation of exciton-biexciton bunching in colloidal QDs. Our low-temperature single-particle measurements show cascaded XX-X emission of single photon pairs for over 200 seconds, with minimal overlap between X and XX features. The X-XX distinguishability allows for an in-depth theoretical characterization of cross-correlation strength, placing it in perspective with photon pairs of epitaxial counterparts. These findings highlight a strong potential of semiconductor quantum shells for applications in quantum information processing.

Introduction.

Non-classical states of light are at the forefront of the emerging quantum optics technologies, with nascent applications in quantum communication,[1,2] information processing,[3,4] sensing,[5] and computation.[6] Significant progress has been made in engineering quantum light sources that emit single photons. Nearly ideal deterministic single-photon emitters can now be realized using epitaxially grown quantum dots (QDs) which benefit from mature semiconductor processing methods and the integration of photonic microcavities to enhance light output and indistinguishability.[7,8,9] Epitaxial QDs have also stimulated research into the on-demand generation of more complex photonic states, such as correlated photon pairs and entangled photon states[10,11,12,13] particularly at cryogenic temperatures where they show great promise for producing entangled pairs.[11,12] However, the fabrication of epitaxial QDs via molecular-beam epitaxy is non-trivial and thus presents significant scalability challenges.

Conversely, colloidal semiconductor quantum dots (CQDs), synthesized via wet-chemical methods, offer a scalable and cost-effective alternative.[14,15,16,17,18,19] However, CQDs suffer from fast non-radiative decay processes, including Auger and surface recombination, that lead to charging, spectral fluctuations of photoluminescence (PL), poor coherence, and PL flickering. These issues severely limit the ability of CQDs to produce distinct emissions from exciton (X) and biexciton (XX) states, thereby hindering their application in generating single photons or entangled photon pairs. Despite these challenges, recent advancements in non-blinking $CsPbBr_3$ and InP CQDs with short radiative lifetimes and spectral stability[19] of XX and X spectral lines have demonstrated photon indistinguishability,[15] sparking a renewed interest to the colloidal nanostructures for quantum information processing.

Here, we demonstrate that colloidal semiconductor quantum shells (QSs)[20,21,22,23,24,25,26] with a CdS_{core}-$CdSe_{shell}$-CdS_{shell} geometry can produce spectrally distinct and stable emission from X and XX states - an essential characteristic of a quantum emitter. This capability has allowed us to observe X and XX photon bunching behavior in QSs - a phenomenon not previously seen in colloidal nanocrystals. The significant spectral separation between X and XX photons, as shown in **Figure 1a**, results from a substantial biexciton binding energy of E_{xx}-E_x = 75-80 meV, attributed to a strong exciton-exciton repulsion within the quantum shell. A combination of a large binding energy and a high biexciton PL QY^{XX} of 50-90% in quantum shells enables the observation of a well-resolved PL trajectory from a XX state with long-term stability exceeding 200 seconds (Figure 1b). Using low-temperature single-particle measurements, we have recorded temporal correlation (photon bunching) between X and XX photons, signifying biexciton cascade relaxation. The experimental realization of clear bunching behavior in QSs has also facilitated a theoretical analysis of the

underlying quantum mechanical processes. By utilizing a three-level system model, we demonstrated that the photon statistics of the cascade can be altered from an asymmetric to a symmetric (spike-like) degree of bunching depending on the number of contributing decay processes. In particular, the model shows a familiar "butterfly" bunching signature when XX and X photons are perfectly separated, transitioning to a symmetric "spike" behavior with increased cross-leakage. Our simulations suggest that the observed bunching, despite visual separation of XX and X lines, is likely affected by some unresolved emission lines contributing to the background, such as charged excitons and higher-order biexcitons. These findings enhance our fundamental understanding of multiphoton emission events and underscore the potential of quantum shells as a promising semiconductor colloidal QD geometry for developing quantum emitters.

Results and Discussion

The generation of correlated photon pairs in semiconductor QDs was originally proposed by Benson et al.[27] by exploiting biexciton (XX) - exciton (X) radiative cascades. This process begins with the decay of the XX state, which involves the recombination of an electron-hole pair and the emission of a single photon, transitioning the QD to a single exciton state. Subsequently, a second emission occurs, allowing the exciton state to relax back to the ground state. Owing to Coulomb interactions, the XX state shows a substantial spectral shift with respect to the case of two unbound excitons. The polarization properties of the emitted photon pair are influenced by the optical properties of the active exciton doublet state. In a symmetric quantum dot, the X states are degenerate, making the emitted photon pairs indistinguishable. However, in more realistic scenarios where the quantum dot is asymmetric or due to the presence of fine structure splitting and exchange interactions, the photons become distinguishable. The resulting quantum cascade emits pairs of photons in two possible decay channels with orthogonal linear polarizations, producing either two horizontally polarized photons or two vertically polarized ones.[28]

In this work, we employed colloidal semiconductor quantum shells as a promising nanoscale geometry for studying the biexciton cascade. Compared to most colloidal nanocrystals, QS structures provide sufficiently high biexciton PL QY and significant spectral separation between XX and X states. **Figure 1a** illustrates the structure of a CdS/CdSe/CdS quantum shell, which consists of a spherical CdSe quantum-well layer sandwiched between two CdS potential barriers. This core/shell/shell morphology is similar to previously reported Quantum-Dot Quantum-Wells (QDQW) nanocrystals but distinguishes itself with a large CdS core component whose size surpasses the exciton Bohr radius. The rationale for using a larger core is to increase the volume of the CdSe shell. By enlarging the CdSe quantum-well volume, Coulomb interactions among multiple excitons are effectively diminished, which in turn reduces their Auger recombination rate.

Electron microscopy images of quantum shells in **Figure 1(d,e)** confirm the presence of three distinct regions within the QS structure: the CdS core, the CdSe quantum-well layer, and the CdS outer shell. The hexagonal morphology of these nanocrystals suggests a thermodynamically driven growth, achieved through high temperature annealing in the presence of unique surfactants (please see the Supplementary Information for details of synthesis). The linear optical absorption and PL emission characteristics of the 6.0-nm core QSs in solution are shown in **Figure 1c**. The PL full width half maximum (FWHM) is 96 meV, which is comparable to that of II-VI quantum dots.

To characterize the spectral properties of exciton and biexciton states in our samples, we start by employing ensemble measurements of amplified spontaneous emission (ASE). This technique provides a direct method for determining the energy separation between the X and XX bands and allows for estimating the average number of electron-hole (*e*-*h*) pairs in specific multi-exciton states by monitoring ASE at varying pump power levels. **Figure 2a** shows a characteristic ASE spectrum from a spincoated film of 6.0-nm-core CdS-CdSe-CdS QSs. Here, the single exciton PL signal is detectable under any level of excitation power, while

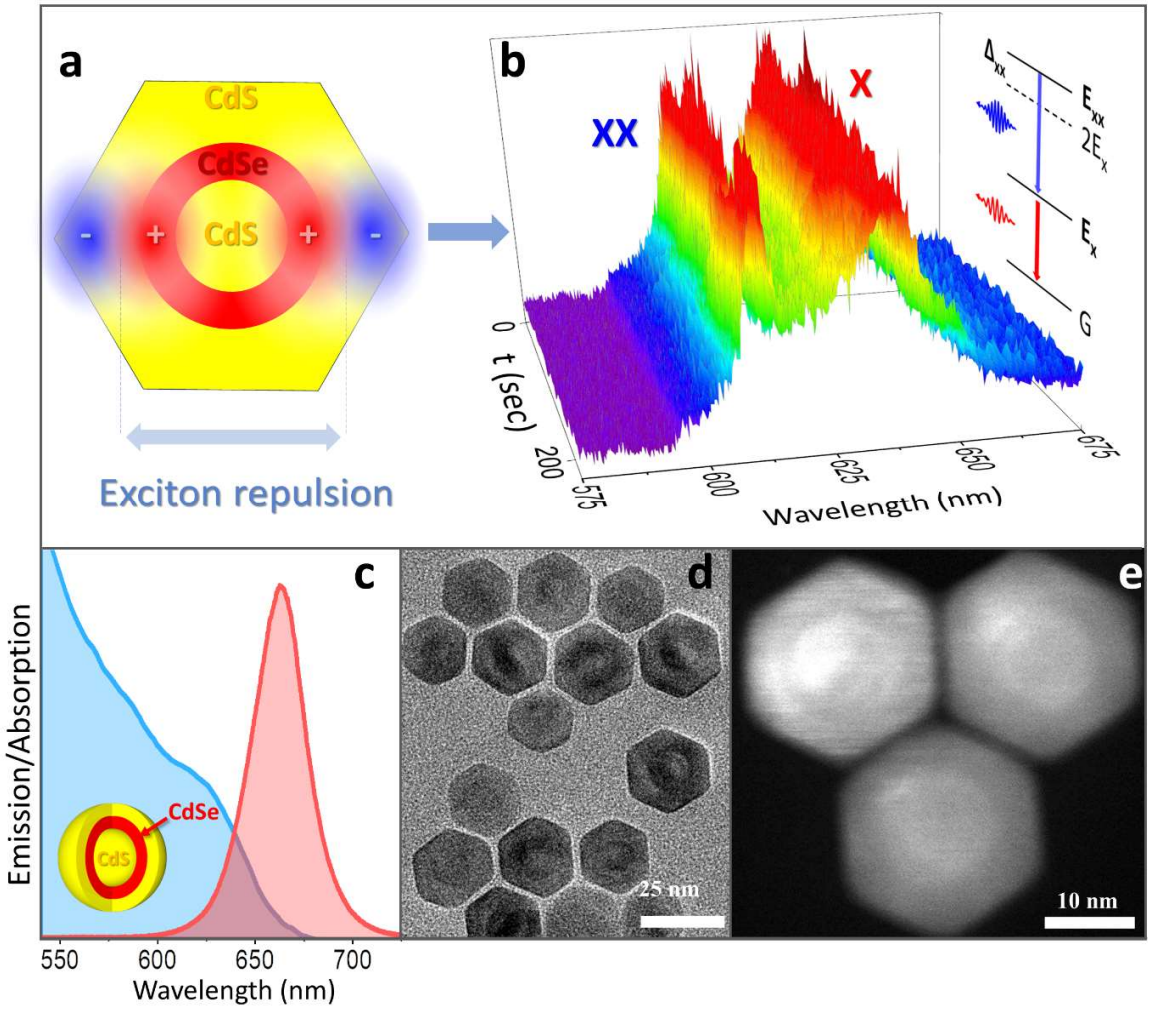

Figure 1. (a) A diagram illustrating exciton-exciton repulsion in a quantum shell structure. (b) Time-dependent PL spectra of an individual QS showing energy-separated X and XX emission bands. The integration time of each frame is 1s. The insert shows an energy diagram of a two-exciton state of a QS. (c) Emission and absorption profiles of a 6.0-nm-core CdS-CdSe-CdS QS. (d) Characteristic TEM image of 6.0-nm-core CdS-CdSe-CdS QSs. (e) High angle annular dark field (HAADF)-STEM images of 6.0-nm-core quantum shells, illustrating the location of the CdSe shell layer.

the XX ASE feature only emerges beyond a specific power threshold. The measured energy gap between the X and XX bands is 78 meV, with the biexciton state residing at a higher energy level. This energetic ordering of X and XX states is unusual because, in both colloidal and epitaxial quantum dots, XX transitions typically exhibit lower energy ($\Delta_{xx} < 0$). In quantum shells, however, exciton-exciton repulsion results in a positive Δ_{xx}, pushing the energy of the XX state above that of the X state. Furthermore, the observed energy difference between the XX and X states in QSs (E_{XX} - E_X) is significantly larger — by a factor of 3-4 —

compared to most colloidal nanocrystals, enabling a clearer spectral distinction between the X and XX emission bands.

To perform single-particle PL at cryogenic temperatures, stock solutions of QSs were diluted and spin-coated onto precleaned quartz substrates. The samples were then loaded into a continuous-flow liquid helium cryostat integrated into a home-built PL setup. Optical excitation of the QSs was achieved using either CW 532 or a pulsed picosecond (ps) 400 nm laser, focused onto the samples with a microscope objective (NA = 0.6, 40× magnification). The pulsed laser delivered pulses approximately 50 ps in duration at a variable repetition rate of between 5-10 MHz. PL emitted from the QSs was collected by the same objective and directed either to a charge-coupled device (CCD) attached to a spectrometer for imaging and spectroscopic analysis or to a pair of single-photon avalanche diodes in a Hanbury Brown-Twiss configuration for time-resolved and time-correlated single photon counting experiments. Optical measurements were conducted either at room temperature or at 10 K, as specified.

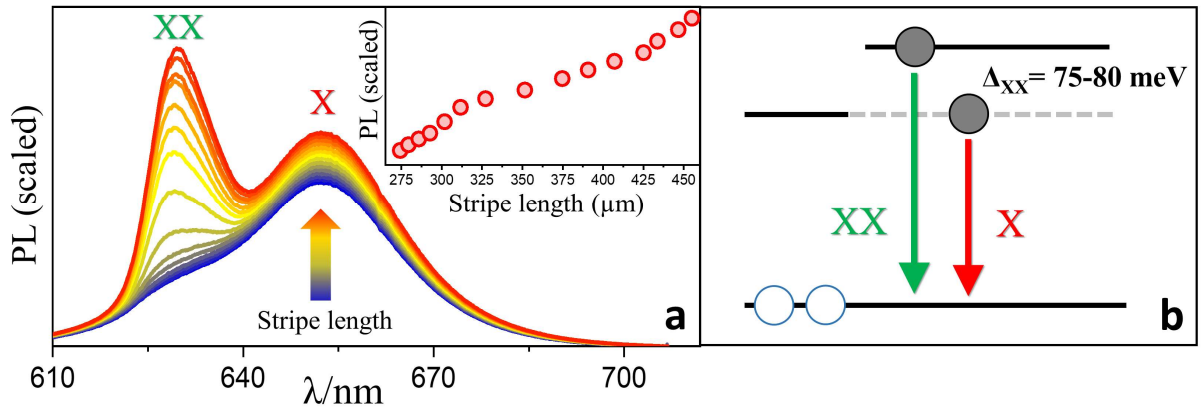

Figure 2. (a) Room temperature PL intensity of a QS thin film at various stripe lengths of the excitation spot. Inset: Integrated intensity of the ASE vs. stripe length. (b) Energy diagram showing the X – XX energy separation corresponding to panel (a).

Quantum shells that exhibit nearly complete Auger suppression are prime candidates for multiphoton generation. Recently, we have shown that CdS/CdSe/CdS QSs exhibit nearly 100% biexciton quantum yield. To study their emission properties, we used both fluorescence intermittency (blinking) and photon correlation techniques to record the behavior of individual 6-nm core CdS/CdSe/CdS QSs at room temperature. Figure SF 3a shows a typical blinking intensity trace of a single QS under pulsed excitation (400 nm and 25 nW), indicating minimal fluorescence intermittency. The absence of blinking in these QSs

has been attributed to suppressed Auger recombination, allowing both charged trions and biexcitons to undergo radiative recombination.

To quantify the XX quantum yield (QY^{XX}) we employed second-order photon correlation measurements ($g^2(\tau)$) as established by Nair et al. Ref[29] This method correlates the value of antibunching function with quantum yield as $g^2(0)=QY^{XX}/QY^{X}$ in the limit of the low pump power. It is particularly suitable for measurements of spectrally inseparable emission lines from XX and X transitions when both types of emissions are simultaneously collected into each arm of the HBT setup. Several recent papers successfully

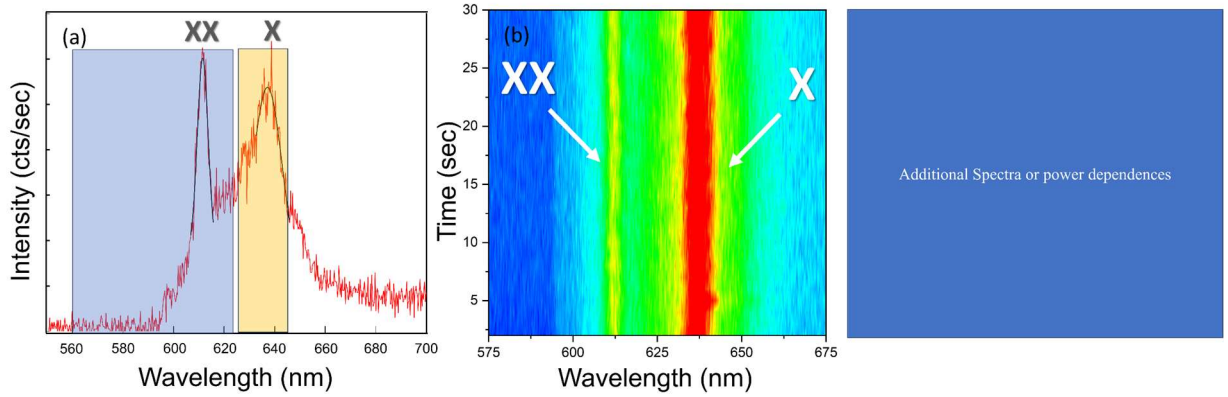

Figure 4: (a) Single QS spectra taken at 10 K. Shaded bars show the bandpass filters used to separate the emission for correlation measurements. (b) 3D plot intensity plot of the same QS taken over 30 sec and indicating the spectral stability of the XX and X lines. (c) Spectra at higher excitation powers (to be added)

demonstrated large QY^{XX} ranging from 40-80 % for large core CdSe/CdS NQDs[30,31] and QSs[25,32] and reach nearly 100 % for 8 nm core CdS/CdSe/CdS QSs. An example is shown in Figure S3b, where $g^2(0)=QY^{BX}$~85 % is demonstrated for 6-nm core QS. To exclude possible mishap with small QS clusters that would also provide non-zero $g^2(0)$ values,[33,34] we applied a variable time gating procedure when calculating $g^2(\tau)$ values. Analyzing $g^2(\tau)$ traces using only photons with decay times longer than that of the biexciton state (τ_{XX} = 5-10 ns for 6.0-nm core QSs),[30,32] we thus excluded biexciton contributions. Figure SF3c shows the $g^2(\tau)$ trace after implementing a gate time of 15 ns, where the $g^2(0)<0.5$ as would be expected for exciton-only contribution. [23,32]

Despite the overall high biexciton quantum yield, emissions from XX and X spectral lines need to be spectrally resolved to fully realize their potential for photon pair generation. **Figure 4a** shows the low-temperature (10 K) integrated spectrum of a single QS acquired with a one-second accumulation time using continuous-wave (cw) 532 nm laser excitation. Until now, spectrally resolved XX and X lines from colloidal nanoparticles have rarely been observed due to low biexciton emission efficiencies.[35] The spectrum reveals two distinct PL bands with an energy separation of 85 meV, representing the XX and X lines at 610 and

637 nm, respectively. Local electrostatic field variations often cause spectral diffusion and linewidth fluctuations in nanocrystals,[36] leading to overlapping emissions and long-term instability. This has hindered their use as stable sources of correlated photon pairs. However, **Figure 4b** demonstrates that QSs exhibit stable long-term photoluminescence over several minutes, comparable to spectral stability of recently reported InP NCs.[19] The stable emission confirms a relatively low density of charged states as previously suggested by the high emission QYs.

To fully evaluate QSs for quantum cascade emission, we performed spectrally resolved photon cross correlation measurements of $g^2(\tau)$ between XX and X emission lines. Leveraging the large spectral separation and long-term emission stability, we employed bandpass interference filters to isolate each emission line, as shown in the shaded areas of **Figure 4a**. **Figure 5(a,b)** shows a scheme of the employed HBT correlation setup with spectral separation of the XX and X lines and resulting photon correlations at two different powers under cw 532 nm laser excitation. A clearly observed bunching signature (*i.e.* $g^2(0)>1$) is seen as a somewhat asymmetric spike at zero delay time for $g^2(\tau)$ function. While such bunching has been seen in various epitaxial QD systems, it has not been observed in colloidal nanocrystals until now, highlighting the unique capabilities of QSs in this context.

The observed bunching in our measurements can be explained by several mechanisms. First, it may be attributed to the spectrally resolved XX-X cascade, where XX photons initiate one of the APD detectors ("Start"), and X photons the other detector ("Stop"), creating a distinct cross-correlation.[28,37,38]

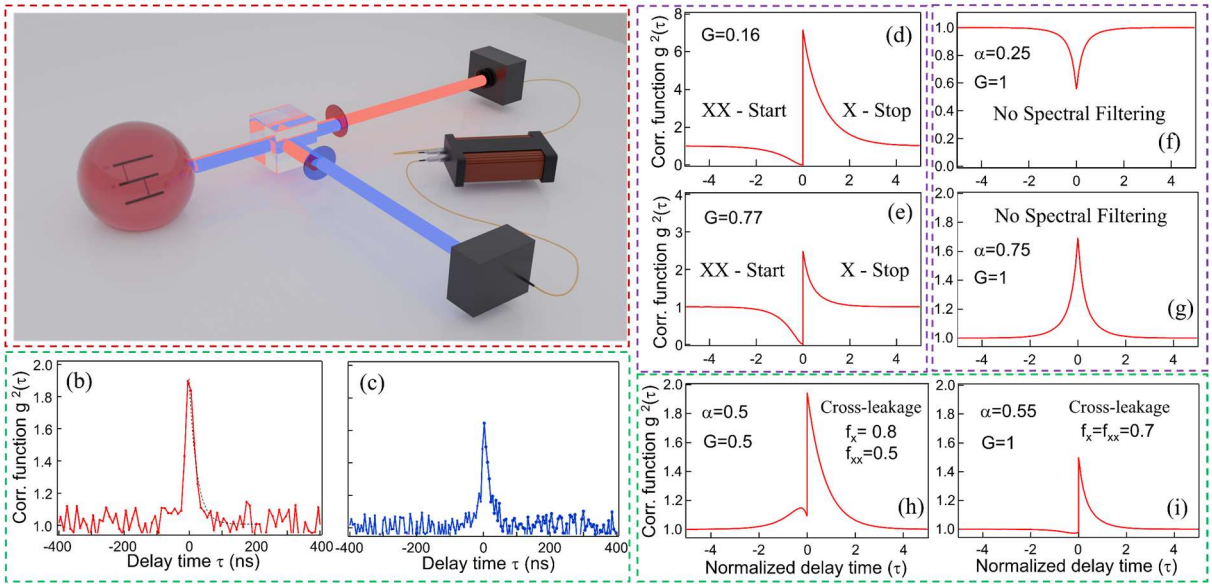

Figure 5. (a) Schematics of radiative XX-X cascade and spectrally resolved correlation measurements. (b,c) Correlation function $g^2(\tau)$ between spectrally isolated XX (start) and X (stop) photons at two excitation powers (excitation wavelength 532 nm). (d,e) simulations of $g^2(\tau)$ function for spectrally separated XX and X emission at two excitation rates G. (f,g) $g^2(\tau)$ for two values of α parameters for spectrally inseparable emission (h,i) simulation of $g^2(\tau)$ for various degrees (f_x and f_{xx}) of emission leakage between X and XX channels at two different excitation power levels G.

Alternatively, this bunching could be the result of spectral diffusion, caused by random fluctuations in the spectral line due to environmental changes, leading to variations in photon emission timing.[39,40] However, recent studies on II-VI systems, specifically those with well-controlled CdSe–CdS and facet–ligand interfaces, have demonstrated that spectral diffusion can be significantly reduced, with variations kept below 110 μeV observed over hours-long periods.[41] This suggests that, in well-engineered systems, spectral diffusion is less likely to be the primary cause of bunching. Yet another plausible explanation is the existence of spectrally unresolved lines, which contribute to a broadband background that underlies both XX and X lines.

To clarify the observed photon correlations in a XX-X system under continuous wave 532 nm laser excitation, we perform numerical simulation of the $g^2(\tau)$ functions. Using a three-level rate equation model with XX, X, and ground states, we examined the effects of spectral separation and imperfect filtering on the $g^2(\tau)$ function. Such a three-level model allows for the analytical solution as presented in Suppl. Information section, with n_2 (t), n_1 (t) and n_0 (t) corresponding to time-evolution of the population of each

state accordingly. In the model, we assumed that XX (X) decay rates k_2 (k_1) are related as $k_2=4k_1$, and the photogeneration rate G under cw excitation conditions is equal for both processes. In the small G limit, this model reduces to one previously studied by Avanaki and Schatz [Kobra N. Avanaki and George C. Schatz, J. Chem. Phys. 154, 024304 (2021). DOI:10.1063/5.0032648) which shows important entanglement effects in the limit $k_2<k_1$, but the entanglement properties of the emitted photons for larger G are not known.]

The second-order correlation function between states labeled *i* and *j* is computed as $g^2_{ij}(\tau)=n^i_j(\tau)/n^{ss}_j$, where $n^i_j(\tau)$ is a population of the state which involves "*i"* e-h pairs and where a photon will be emitted at time τ after such an emission which involves "*j"* pairs has previously occurred. Also, n^{ss}_j corresponds to the steady-state solution of the *j*-state.[42,43] Obviously, when the same spectral line is monitored on the both channels (*i*=*j*), this equation turns into the second-order antibunching function. Additionally, we correct for non-ideal spectral separation of photons into each detector channel, either due to imperfect filters that allow cross-leakage of photons or due to existence of other XX (X)-like emission lines unaccounted for in the spectra.

When XX and X photons are fully spectrally separated using perfect filters and detected in the appropriate channels—where the Start signal is from XX photons and the Stop signal is from X photons—the $g^2(\tau)$ function typically displays a "butterfly"-like bunching signature. This pattern corresponds to cascaded emission, as demonstrated in **Figure 5(d,e)**.[38,44] The amplitude of this bunching signature decreases at higher excitation powers, a behavior that aligns with our simulation results.[45] Although our experimental data exhibit a similar power dependence, the graphs in **Figure 5(b,c)** do not show the expected butterfly-like behavior of the $g^2(\tau)$ function.

A crossover from asymmetric "butterfly" bunching to symmetric "spike" like behavior has been previously seen in epitaxial QD systems with unusually broad XX and X emission lines.[46] This occurs when all photons reach each detector, meaning the (XX+X) signal is detected without spectral filtering. In such cases, the recorded $g^2(\tau)$ function is essentially a sum of all possible correlations, represented as $g^2(\tau) = \Sigma(g^2_{ij}(\tau))$ for *i*=1,2 and *j*=1,2, where XX is denoted as "2" and X as "1". This summation includes contributions from pure antibunching terms $g^2_{11}(\tau)$ and $g^2_{22}(\tau)$, which range between 0 and 1, as well as cross-correlation terms $g^2_{21}(\tau)$ and $g^2_{12}(\tau)$, which exhibit large bunching components at small delay times τ. We can define a proportion of each of the individual contributions as: $g^2(\tau)=\alpha g^2_{21}(\tau)+\beta g^2_{12}(\tau)+\gamma g^2_{11}(\tau)+\delta g^2_{22}(\tau)$, where α, β, γ, δ are "generation" parameters that vary from 0 to 1 and $\alpha+\beta+\gamma+\delta=1$, see Suppl. Information for full description of the model.[47] These parameters would be related to steady-state populations of X and XX states at a given pump rate G and the corresponding probabilities to detect a photon from an "*i*" state once the emission from "*j*" has occurred.

For small α values, the $g^2(\tau)$ function is mainly influenced by antibunching terms, resulting in a symmetric function that dips below value of 1. As α increases, the function shifts to a symmetric "spike"-like bunching signature. Our simulation data in **Figure 5(f, g)** confirm this behavior, showing that the $g^2(\tau)$ function is dominated by antibunching for small α and transitions to symmetric bunching for larger α. This crossover is highly dependent on the exact set of generation parameters, which are a function of the pumping power, as detailed in Supplementary Information Figure Sxx. Regardless of the parameter set, the $g^2(\tau)$ signature remains symmetric, highlighting the robustness of this behavior across different conditions.

In reality, neither of the idealized scenarios fully explains the observed bunching behavior. While the XX and X lines in the spectra (**Figure 4**) appear sufficiently separated, the X line does leak into the XX detection channel, as indicated by fitting of the emission lines. More critically, both lines sit atop a much broader "pedestal" background emission that contributes to both channels. The exact origin of this background is unclear, but it is likely due to unresolved emission lines such as charge excitons (trions) or higher-order biexcitons, including $1S_e$-$2S_h$ transitions. This is supported by spectra taken at higher power (**Figure 4c**), which show the emergence of additional emission lines between X and XX, affecting both detector channels.

To account for these complexities, we introduced filter transmission parameters into our model to simulate partial leakage of the signal across channels. By keeping other parameters constant and varying these filter transmission parameters to represent the cross-leakage of X-like emission into the XX detection channel and vice versa, we were able to closely replicate the appearance of the asymmetric-spike like bunching features and their dependence on pump power, **Figure 5(h,i)**. This approach demonstrates that the observed bunching behavior can be accurately modeled by considering the leakage and background contributions, providing a more comprehensive understanding of the photon correlation dynamics in our system.

The above considerations qualitatively explain the general features of the observed XX-X correlations. Despite the visual separation of the XX and X lines, their mutual cross-correlation exhibits atypical bunching. This behavior, while still indicative of the XX-X cascade, suggests that other emission lines are also contributing to the detection channels. At low temperatures, colloidal QDs often exhibit enhanced charging rates due to mechanisms like surface charge trapping or Auger ionization, which lead to charged exciton emission. The dynamic trapping and de-trapping of these additional charges within a QD cause rapid switching between biexciton-exciton and charged exciton emissions. This rapid switching introduces additional complexity to the emission spectra, contributing to the observed bunching in the cross-correlation data. Therefore, while the XX-X cascade is a primary factor, the presence of charge excitons and other emission lines must be considered to fully understand the photon correlation dynamics.

In conclusion, we demonstrate that biexciton-exciton cascade decay in colloidal semiconductor quantum shells can yield spectrally distinct and temporally stable photon pairs. This unique capability has enabled the observation of X and XX bunching behavior, a phenomenon not previously seen in colloidal QDs. Low-temperature single-particle measurements have confirmed the temporal correlation between X and XX photons, indicative of biexciton cascade relaxation. Our theoretical analysis, supported by a three-level system model, shows that the photon statistics of the cascade can transition from an asymmetric "butterfly" to a symmetric "spike" behavior depending on the degree of cross-leakage. These findings highlight the significance of unresolved emission lines and background contributions, enhancing our understanding of multiphoton emission events and reinforcing the potential of QSs as promising candidates for quantum emitters in quantum information processing. Overall, the ability to reliably produce and manipulate photon pairs or employ spectrall filtering to achieve single-photon emission highlights the potential of quantum shells as quantum light sources.

Acknowledgement. The work of the BGSU team was supported by the award DE-SC0016872 (MZ). DH and MZ acknowledge the support by NSF award #2208834. GCS was supported by NSF award # 2347622.

Supporting Information. QS synthesis, fabrication of nanopillar arrays, calculations of absorption cross-section. Available free of charge at https://pubs.acs.org/doi

References

[1] R.M. Stevenson et al., A semiconductor source of triggered entangled photon pairs. Nature 439, 179–182 (2006)
[2] Chip-integrated visible–telecom entangled photon pair source for quantum communication, Nat. Phys. 15, 4 (2019).
[3] R.M. Stevenson et al., A semiconductor source of triggered entangled photon pairs. Nature 439, 179–182 (2006)
[4] C.-Y. Lu, J.-W. Pan, Quantum-dot single-photon sources for the quantum internet. Nat. Nanotechnol. 16, 1294–1296 (2021)
[5] X. Guo et al., Distributed quantum sensing in a continuous variable entangled network, Nat. Phys. 16, 281 (2020).
[6] L. S. Madsen et al., Quantum computational advantage with a programmable photonic processor, Nature (London) 606,

7912 (2022).
[7] M. Pelton et al., Efficient source of single photons: a single quantum dot in a micropost microcavity. Phys. Rev. Lett. 89, 233602 (2002)
[8] P. Senellart, G. Solomon, A. White, High-performance semiconductor quantum-dot single-photon sources. Nat. Nanotechnol. 12, 1026–1039 (2017)
[9] H. Wang et al., Towards optimal single-photon sources from polarized microcavities. Nat. Photonics 13, 770–775 (2019)
[10] C.L. Salter et al., An entangled-light-emitting diode. Nature 465, 594–597 (2010)
[11] M. Müller, S. Bounouar, K.D. Jöns, M. Glässl, P. Michler, On-demand generation of indistinguishable polarization-entangled photon pairs. Nat. Photonics 8, 224–228 (2014)
[12] H. Wang et al., On-demand semiconductor source of entangled photons which simultaneously has high fidelity, efficiency, and indistinguishability. Phys. Rev. Lett. 122, 113602 (2019)
[13] Mechanistic understanding of entanglement and heralding in cascade emitters J. Chem. Phys. 154, 024304 (2021);
[14] J.M. Pietryga et al., Spectroscopic and device aspects of nanocrystal quantum dots. Chem. Rev. 116, 10513–10622 (2016)
[15] H. Utzat et al., Coherent single-photon emission from colloidal lead halide perovskite quantum dots. Science 363, 1068–1072 (2019)
[16] X. Lin et al., Electrically-driven single-photon sources based on colloidal quantum dots with near-optimal antibunching at room temperature. Nat. Comm. 8, 1132 (2017)
[17] Superior optical properties of perovskite nanocrystals as single photon emitters. ACS Nano 9, 12410–12416 (2015)
[18] Y.-S. Park, S. Guo, N.S. Makarov, V.I. Klimov, Room temperature single-photon emission from individual perovskite quantum dots. ACS Nano 9, 10386–10393 (2015)
[19] Proppe, A.; Berkinsky, D. B.; Zhu, H.; Sverko, T.; Kaplan, A. E. K.; Horowitz, J. R.; Kim, T.; Chung, H.; Jun, S.; Bawendi, M. G. Highly stable and pure single-photon emission with 250 ps optical coherence times in InP colloidal quantum dots, *Nature Nanotech.* **2023** 18(9), 993-999

[20] N. Razgoniaeva, P. Moroz, M. Yang, D. S. Budkina, H. Eckard, M. Augspurger, D. Khon, A. N. Tarnovsky, M. Zamkov, One-Dimensional Carrier Confinement in "Giant" CdS/CdSe Excitonic Nanoshells, *J. Am. Chem. Soc.*, 2017, **139**, 7815–7822.

[21] N. Kholmicheva, D. S. Budkina, J. Cassidy, D. Porotnikov, D. Harankahage, A. Boddy, M. Galindo, D. Khon, A. N. Tarnovsky and M. Zamkov, Sustained Biexcitonic Populations in Nanoshell Quantum Dots, *ACS Photonics*, 2019, **6**, 1041–1050.

[22] G. Nagamine, B. G. Jeong, T. A. C. Ferreira, J. H. Chang, K. Park, D. C. Lee, W. K. Bae and L. A. Padilha, Efficient Optical Gain in Spherical Quantum Wells Enabled by Engineering Biexciton Interactions, *ACS Photonics*, 2020, **7**, 2252–2264.

[23] J. Cassidy, B. T. Diroll, N. Mondal, D. B. Berkinsky, K. Zhao, D. Harankahage, D. Porotnikov, R. Gately, D. Khon, A. Proppe, M. G. Bawendi, R. D. Schaller, A. V. Malko and M. Zamkov, Quantum Shell Boost the Optical Gain of Lasing Media, *ACS Nano*, 2022, **16**, 3017–3026.

[24] A. H. Proppe, K. L. K. Lee, C. L. Cortes, M. Saif, D. B. Berkinsky, T. Sverko, W. Sun, J. Cassidy, M. Zamkov, T. Kim, E. Jang, S. K. Gray, B. A. McGuire and M. G. Bawendi, Adversarial autoencoder ensemble for fast and probabilistic reconstructions of few-shot photon correlation functions for solid-state quantum emitters *Phys. Rev. B*, 2022, **106**, 045425.

[25] J. Cassidy, D. Harankahage, D. Porotnikov, A. V. Malko and M. Zamkov, Colloidal Quantum Shells: An Emerging 2D Semiconductor for Energy Applications, *ACS Energy Lett.*, 2022, **7**, 1202–1213.

[26] Harankahage, D., Cassidy, J., Beavon, J., Huang, J., Brown, N., Berkinsky, D., Zhang, K., Anzenbacher, P., Schaller, R., Sun, L., Bawendi, M., Malko, A., Diroll, B., Zamkov. M. Quantum Shell in a Shell:

Engineering Colloidal Nanocrystals for a High-Intensity Excitation Regime, *J. Am. Chem. Soc*., **2023** *145*, 13326–13334.

[27] Benson, O., Santori, C., Pelton, M., Yamamoto, Y. Regulated and Entangled Photons from a Single Quantum Dot., *Phys. Rev. Lett*., **2000**, *84*, 2513-2516.
[28] Santori, C., Fattal, D., Pelton, M., Solomon, G. S., Yamamoto, Y. Polarization-correlated photon pairs from a single quantum dot. *Phys. Rev. B*., **2002**, *66*, 045308
[29] Nair, G.; Zhao, J.; Bawendi, M. G. Biexciton Quantum Yield of Single Semiconductor Nanocrystals from Photon Statistics. *Nano Lett*. **2011**, 11, 1136−1140.
[30] Mangum, B. D.; Sampat, S.; Ghosh, Y.; Hollingsworth, J. A.; Htoon, H.; Malko, A. V. Influence of the Core Size on Biexciton Quantum Yield of Giant CdSe/CdS Nanocrystals, *Nanoscale* **2014, 6 (7), 3712 – 3720**
[31] Sampat, S.; Karan, N. S.; Guo, T.; Htoon, H.; Hollingsworth, J. A.; Malko, A. V. Multistate Blinking and Scaling of the Recombination Rates in Individual Silica-Coated CdSe/CdS Nanocrystals, *ACS Photonics* **2015,** 2 (10), 1505-1512
[32] Marder, A. A.; Cassidy, J.; Harankahage, D.; Beavon, J.; Gutiérrez-Arzaluz, L.; Mohammed, O. F.; Mishra, A.; Adams, A. C.; Slinker1, J. D.; Hu, Z.; Savoy, S.; Zamkov, M.; Malko, A. V. CdS/CdSe/CdS Spherical Quantum Wells with Near-Unity Biexciton Quantum Yield for Light-Emitting Device Applications. ACS Materials Lett. 2023, 5, 1411–1419.
[33] Bussian, D. A.; Malko, A. V.; Htoon, H.; Chen, Y.; Hollingsworth, J. A.; Klimov, V. I. Quantum Optics with Nanocrystal Quantum Dots in Solution: Quantitative Study of Clustering. *J. Phys. Chem. C*. **2009**, 113, 2241-2246
[34] Mets, Ü. Antibunching and rotational diffusion in FCS. (Springer, Berlin Heidelberg, 2001).
[35] Peng, L.; Cho, W.; Zhang, X.; Talapin, D, Ma, X., Observation of Biexciton Emission from Single Semiconductor Nanoplatelets. *Phys. Rev. Mater*. **2021**, 5, L051601
[36] S. A. Empedocles and M. G. Bawendi, Science 278, 2114 (1997).
[37] A. Malko, D. Y. Oberli, M. H. Baier, E. Pelucchi, F. Michelini, K. F. Karlsson, M.-A. Dupertuis, and E. Kapon, Single photon emission from pyramidal quantum dots: The impact of hole thermalization on photon emission statistics, *Phys. Rev. B* **72**, 195332 (2005)
[38] M. H. Baier, A. Malko, E. Pelucchi, D. Y. Oberli, and E. Kapon, Quantum dot exciton dynamics probed by photon correlation spectroscopy, *Phys. Rev. B* **73**, 205321 (2006)
[39] G. Sallen, A. Tribu, T. Aichele, R. Andre, L. Besombes, C. Bougerol, M. Richard, S. Tatarenko, K. Kheng and J.-Ph. Poizat, Subnanosecond spectral diffusion measurement using photon correlation, *Nat. Phot.* **2010**, *4*, 696-699
[40] W. Walden-Newman, I. Sarpkaya, and S. Strauf, Quantum Light Signatures and Nanosecond Spectral Diffusion from Cavity-Embedded Carbon Nanotubes, *Nano Lett*. **12**, 1934 (2012).
[41] 10.1021/acs.nanolett.3c04250
[42] Regelman, D. V.; Mizrahi, U. Gershoni, D.; Ehrenfreund, E., Semiconductor Quantum Dot: A Quantum Light Source of Multicolor Photons with Tunable Statistics. *Phys. Rev. Lett*. **2001**, 87, 257401
[43] Fischer, B.; Caruge, J. M.; Zehnder, D.; Bawendi, M. G., Room-Temperature Ordered Photon Emission from Multiexciton States in Single CdSe Core-Shell Nanocrystals, *Phys. Rev. Lett*. **2005**, 94, 087403
[44] Persson, J.; Aichele, T.; Zwiller, V.; Samuelson, L.; Benson, O., Three-photon Cascade from Single Self-Assembled InP Quantum Dots, *Phys. Rev. B* **2004**, 69, 233314
[45] Kuroda, T.; Belhadj, T.; Abbarchi, M.; Mastrandrea, C.; Gurioli, M.; Mano, T.; Ikeda, N.; Sugimoto, Y.; Asakawa, K.; Koguchi, N.; Sakoda, K.; Urbaszek, B.; Amand, T.; Marie, X., Bunching Visibility for Correlated Photons from Single GaAs Quantum Dots, *Phys. Rev. B*, **2009**, 79, 035330
[46] Callsen, G.; Carmele, A.; Honig, G.; Kindel, C.; Brunnmeier, J.; Wagner, M. R.; Stock, E.; Reparaz, J. S.; Schliwa, A.; Reitzenstein, S.; Knorr, A.; Hoffman, A.; Kako, S.; Arakawa, Y., Steering Photon Statistics in Single Quantum Dots: From One- to Two-Photon Emission, *Phys. Rev. B*, **2013**, 87, 245314

[47] Heindel, T.; Thoma, A.; von Helversen, M.; Schmidt, M.; Schlehahn, A.; Gschrey, M.; Schnauber, P.; Schulze, J.-H.; Strittmatter, A.; Beyer, J.; Rodt, S.; Carmele, A.; Knorr, A.; Reitzenstein, S. A Bright Triggered Twin-Photon Source in the Solid State, *Nat. Comm*., **2017**, 8, 14870